Supplementary Information (SI) for Energy & Environmental Science.
This journal is © The Royal Society of Chemistry 2025

Electronic Supporting Information

Achieving 19.6% efficiency in organic photovoltaics through guest-polymer assisted morphological fibrillization

Zhenye Li,[a,b] Jiefeng Xie,[b] Wenquan Wang, [b] Zhiyuan Yang,[a] Lixuan Kan,[c] Ming Zhang,[c] Zaiyu Wang,[d] Wenyu Yang,[a] Feng Peng,[a] Wenkai Zhong,[, a] and Lei Ying*[, a]*

[a] Institute of Polymer Optoelectronic Materials and Devices, Guangdong Basic Research Center of Excellence for Energy & Information Polymer Materials, State Key Laboratory of Luminescent Materials and Devices, South China University of Technology, Guangzhou, 510640 China
E-mail: wkzhong@scut.edu.cn; msleiying@scut.edu.cn

[b] College of Mechanical Engineering, University of South China, Hengyang 421001, China

[c] Frontiers Science Center for Transformative Molecules, Center of Hydrogen Science, and School of Chemistry and Chemical Engineering, Shanghai Jiao Tong University, Shanghai 200240, China

[d] Department of Chemistry and the Hong Kong Branch of the Chinese National Engineering Research Center for Tissue Restoration and Reconstruction, The Hong Kong University of Science and Technology, Clear Water Bay, Kowloon, Hong Kong 999077, China

Experimental Section

Materials

PTzBI-dF, D18, L8-BO, and PFN-Br were procured from Volt-Amp Optoelectronics Tech. Co., Ltd. PBDB-T, PM6, and ITIC were purchased from Nanjing Zhiyan Technology Inc. Ltd. Chloroform (CF), chlorobenzene (CB), o-dichlorobenzene (o-DCB), methanol, 1-chloronaphthalene (1-CN), 1,8-diiodooctane (DIO), and dibenzyl ether (DBE) were sourced from Sigma-Aldrich. All materials were used as received without further purification.

Fabrication and characterizations of OPVs

Indium tin oxide (ITO)-coated transparent glasses were sequentially cleaned with deionized water, isopropanol, and ethanol in an ultrasonic cleaner, then dried at 60 °C before use. The ITO glass substrates were treated with oxygen plasma for 3 minutes and then spin-coated with a PEDOT:PSS solution (Clevios PVP Al 4083) at 3000 rpm for 30 seconds. The coated substrates were subsequently annealed at 150 °C for 15 minutes on a hot plate. Following this, the PEDOT:PSS-coated ITO glasses were transferred to a glove box with a nitrogen environment. For D18:PTzBI-dF:L8-BO active layers, the total concentration of mixture solution was 9.5 mg mL^{-1}. The active layers were prepared by spin-coating the solutions in chloroform (CF) with 0.5 vol% 1-chloronaphthalene (CN) at 3000 rpm for 20 seconds. For PM6:PTzBI-dF:L8-BO active layers, the total concentration was 10 mg mL^{-1}, also using the CF and CN solution as processing solvent and additive, respectively. For PBDB-T:PTzBI-dF:ITIC active layers, the total concentration is 16 mg mL^{-1} in chlorobenzene (CB) with 0.5 vol% 1,8-diiodooctane (DIO). The thickness of these active layers was about 100 nm. The resulting active layers were then thermally annealed at 100 °C for 5 minutes, followed by the spin-coating of a PFN-Br interfacial layer (dissolved in methanol) at 2000 rpm for 30 seconds. Finally, a 100 nm thick silver electrode was deposited on PFN-Br using vacuum thermal evaporation at a pressure of 1×10^{-4} Pa. The active area of devices was 0.0516 cm^2. The illuminated area of device was further defined as 0.04

cm^2 using a square metal aperture. The *J-V* curves were measured using a Keithley 2450 source meter under an AM 1.5 G solar simulator (Zolix Instruments, Sirius-SS150A, 150W AAA grade). The EQE curves were measured using a custom-built EQE system (Zolix, China), equipped with a standard Si diode. The measurements were conducted over a wavelength range of 300-1000 nm, with a step size of 5 nm.

Transient photovoltage (TPV) curves of OPV devices under different light intensities were measured using the PAIOS platform (FLUXiM, Switzerland). The illumination was provided by a white LED light source, with a pulse length of 500 μs and a settling time of 5.00 ms. The light intensity was varied over a range of relative sweep light intensities (1.00%, 1.67%, 2.78%, 4.64%, 7.74%, 12.9%, 21.5%, 35.9%, 59.9%, 100%), enabling the differentiation of resultant device voltage. The illuminated device area was 0.0516 cm^2. The achieved TPV curves and corresponding voltage values at each light intensity are summarized in Fig. S8. Specifically, the fitted lifetimes (τ) as a function of device voltage (V_{OC}) are shown in Fig. S8d. The extracted charge carrier density (n) was measured by charge extraction (CE) method, with the same LED light source and relative sweep light intensity. The extraction duration was 50.0 μs. The τ-n relationship was analyzed using the equation of $\tau = \tau_0(\frac{n_0}{n})^{\lambda}$. The exponent factor λ was obtained by linear fitting of the double-logarithmic plot with $\log(\tau) = -\lambda\log(n) + \lambda\log(n_0)$. For this, the recombination order (R) was calculated by $R = \lambda + 1$, while the recombination rate coefficient ($k(n)$) was determined by $k(n) = \frac{1}{\tau(n) \times n}$.

Impedance spectra of OPV devices were measured in the dark at room temperature with a -0.5 V bias and AC current applied to the device, using the Interface 1010E electrochemical workstation (Gamry Instrument, US) at a frequency range of 0.01 Hz to 100 kHz.

Fabrication of flexible OPVs

The ITO-coated polyethylene glycol terephthalate (PET) flexible substrate was cleaned by wiping with ethanol, and then pre-treated by exposing to oxygen plasma for 3 minutes. PEDOT:PSS (Clevios PVP Al 4083) was spin-coated onto ITO at 3000 rpm

for 30 seconds. After thermal annealled at 80 °C for 15 min, the substrates were transferred into a glove box with a nitrogen environment. For the D18:PTzBI-dF:L8-BO active layers, the total concentration was 9.5 mg mL^{-1}. The active layers were deposited by spin-coating the solutions in CF with 0.5 vol% CN, resulting in a film thickness of about 100 nm. The resulting active layers were then thermally annealed at 100°C for 5 minutes, followed by the spin-coating of a PFN-Br interfacial layer. Finally, a 100 nm thick silver electrode was deposited on PFN-Br using vacuum thermal evaporation at a vacuum level of 1×10^{-4} Pa.

Fabrication and characterization of charge-only devices

Hole and electron mobilities were measured using hole- and electron-only devices, with the structures of ITO/PEDOT:PSS/active layer/Ag and ITO/ZnO/active layer/PFN-Br/Ag, respectively. The dark *J-V* curves were obtained by a Keithley 2450 source meter. Mobilities were extracted using the space-charge-limited current (SCLC) method through the Mott-Gurney relationship $J = 9\varepsilon_r\varepsilon_0\mu V^2/8L^3$, where J is the current density, ε_r is the relative dielectric constant, ε_0 is the vacuum permittivity, μ is the mobility, V is the effective voltage, and L is the thickness of active layer.[1] Here, we used applied volatage as V for the calculation.

Thin film characterizations

The UV-vis-NIR absorption and photoluminescence (PL) spectra were measured using an absorption PL spectral analysis system (APL-AS,IIBiaoQi Optoelectronics). The thin films (~100 nm) were prepared by spin-coating chloroform solutions onto quartz plates for the measurements. The raw data of the absorption spectra were normalized by setting the baseline (~1000 nm) to 0 and the absorption maximum to 1 to eliminate the impact of film thickness.

Time resolved photoluminescence (TRPL) was measured with a Fluorescence lifetime spectrometer (Picoquant, Germany). The thin films (~100 nm) were prepared by spin-coating chloroform solutions onto quartz plates (1 cm × 1cm) for the

measurements. The excitation wavelength was set to 637.4 nm, with a bandpass of 2.4 nm, using a PDL 820 pulsed laser source. The excitation intensity was calibrated to 53% of the maximum power. The detection system used a UV-red PMT detector, with a detection wavelength of 740 nm. The polarization of the detection system was set to 54.7°, and the lens position was at 9.5 mm. The measurements were carried out at a resolution of 25 ps per bin, with a total measurement time of 5.1 seconds. The measurement stopped once the signal reached 10000 counts. The time synchronization was provided by the PDL 820 source with a sync frequency of 10 MHz. The signals were processed using a TimeHarp 260 photon counter with specific signal processing settings, including CFD level of −130 mV and a sync CFD level of -150 mV.

For transient absorption spectroscopy (TA), the output of the Yb:KGW laser (1030 nm, 220 fs Gaussian pulse, 100 kHz, Light Conversion Ltd.) was split into two beams. One beam was directed into the NOPA (ORPHEUS-N, Light Conversion Ltd.) to generate pump light at specific wavelengths (520 nm and 800 nm, with a pulse duration of 30 fs), while the other beam was focused onto a YAG plate to produce a white light continuum as the probe beam. The pump and probe beams were overlapped on the sample at a small angle (<10°). The transmitted probe light was collected using a linear CCD array. The exciton diffusion length (L_D) was estimated using the method outlined in a previous study.[2,3]

Grazing incidence wide angle X-ray scattering (GIWAXS) was conducted using a Xenocs Xeuss 2.0 system equipped with an Excillum MetalJet-D2 X-ray source, operated at 70.0 kV and 2.8570 mA. The incident X-ray had a wavelength of 1.341 Å. All thin films were spin-coated on PEDOT:PSS-coated silicon wafers using the same processing conditions as those for OPV device fabrication. The X-ray beam was directed at an incidence angle of 0.20° to probe the bulk structures. The sample-to-detector distance was set to 210.78 mm, and the scattering pattern was recorded using a DECTRIS PILATUS3 R 1M area detector with exposure time of 30 min. Data reduction and analysis were conducted using the Igor-based Nika package, with in-

plane (IP) and out-of-plane (OOP) I-q curves averaged within sectors at azimuthal angles of 10° and 80°, respectively, each with an angular width of 10°.[4]

Resonant soft X-ray scattering (RSoXS) was conducted at beamline 11.0.1.2 of the Advanced Light Source (ALS), Lawrence Berkeley National Laboratory (LBNL). The thin films were spin-coated on PEDOT:PSS-coated silicon wafers with the same processing conditions used for OPV fabrication. The films were floated on deionized water to dissolve the PEDOT:PSS layer and then transferred onto silicon nitride windows for scattering experiments conducted in transmission mode. The C K-edge NEXAFS spectra of neat films were measured with total electron yield (TEY) mode, with X-ray electric field horizontally polarized to the film surface. Then, the complex refractive indices, absorptive component β, was calcuated by $\beta = \mu/2k$, where μ denotes the attenuation coefficient and k is the wave vector. The dispersive component δ was then obtained via Kramers-Kronig transformation with β. The resultant δ and β of neat materials were used to calculate the contrast funciton $E^4(\Delta\delta^2 + \Delta\beta^2)$. For scattering, the X-ray energy was scanned at C K-edge (280.0, 283.8, 284.2, 284.4, 285.0, 285.2, 285.4, 285.6, 286.0 eV). The X-ray electric field was kept horizontally polarized. Each scattering image was captured using a Princeton Instrument PI-MTE CCD camera with a pixel size of 0.027 mm × 0.027 mm and an exposure time of 5 seconds. The high-q range data (0.004-0.075 $Å^{-1}$) and low-q range data (0.001-0.02 $Å^{-1}$) were collected with sample-to-detector distance of 150 mm and 50 mm, respectively. RSoXS data reduction was carried out using the Igor-based Nika package, with the I-q curves averaged circularly. The final I-q curves were obtained by combining the high-q and low-q data.

Transmission Electron Microscopy (TEM) images were collected using a JEM-2100F transmission electron microscope operated at 200 kV. The thin films were spin-coated onto PEDOT:PSS-coated silicon wafers using the same processing conditions as those for OPV fabrication. The films were then floated on deionized water to dissolve the PEDOT:PSS layer and transferred onto a 300 mesh copper grid.

The Contact angle tests were conducted with a Dataphysics OCA40 Micro surface contact angle analyzer, to determine the water and oil (glycerol) contact angles (θ) for

D18, PTzBI-dF and L8-BO neat films. The thin films (~100 nm) were prepared by spin-coating chloroform solutions onto PEDOT:PSS-coated ITO glasses (1.5 cm × 1.5 cm) for the measurements.

IR spectra and AFM-IR images were measured by Anasys nanoIR3 (Bruker). All films were prepared by spin-coating chloroform solutions onto silicon wafers (1 cm × 1 cm) for the measurements. The IR measurements covered a wavelength range of 780-1800 cm^{-1}, with a spectral resolution of 2 cm^{-1}. AFM-IR images of the D18:L8-BO and D18:PTzBI-dF:L8-BO films were probed at 1430 cm^{-1}.

Additional Figures and Tables

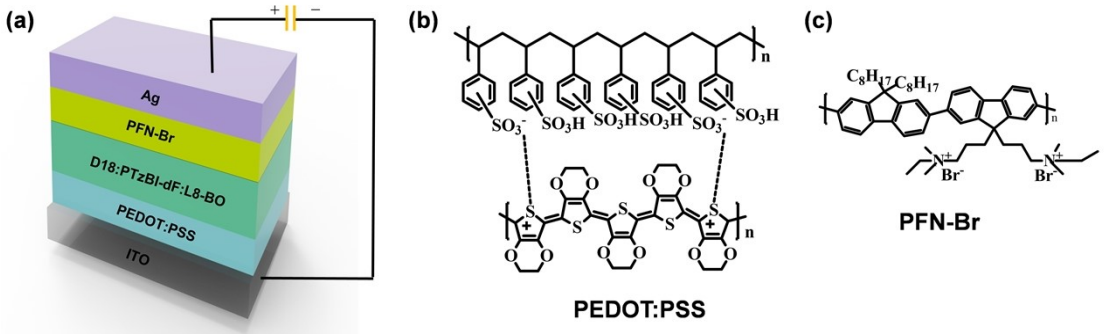

Fig. S1. (a) OPV Device structure used in this work. Chemical structures of (b) PEDOT:PSS and (c) PFN-Br.

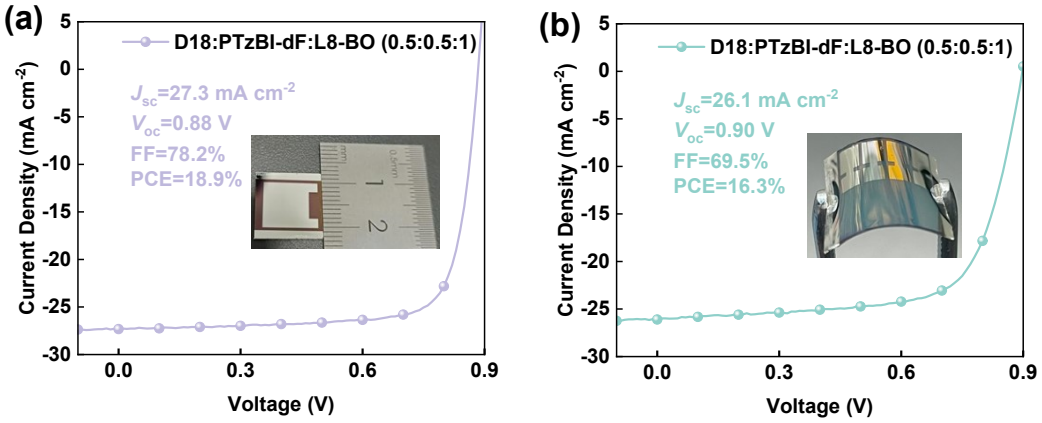

Fig. S2. *J-V* curves of D18:PTzBI-dF:L8-BO (0.5:0.5:1) (a) 1 cm^2 large-area and (b) flexible OPV devices.

合肥广测产品检测研究所
HEFEI GUANGCE PRODUCT TESTING INSTITUTE

测 试 报 告
TEST REPORT

样品名称	大面积有机光伏器件
Name of Sample	Large-area organic photovoltaics
委托单位	华南理工大学
Entrustment Company	South China University of Technology
测试类别	委托验证
Kind of Test	Certification by commission
报告编号	GC202411220013
Report Number	GC202411220013

合肥广测产品检测研究所有限公司

Hefei Guangce Product Test Institute Co., Ltd.

分析测试专用章

中国-合肥 瑶海区包公大道与大众路尚荣大健康产业园 16 栋 D 座 103. 203
咨询电话：400-883-1960 13033058150

测 试 报 告

TEST REPORT

样品名称 Name of Sample	大面积有机光伏器件 Large-area organic photovoltaics	型号/规格 Model/Type	/
样品编号 Sample Number	Y202411160011	测试类别 Kind of Test	委托验证 Certification by commission
委托单位 Entrustment Company	华南理工大学 South China University of Technology		
相关单位 Relative Customer	——		
到样日期 Date of Sample Received	2024.11.16	样品数量 Amount of Sample	1
样品状态描述 Description of Sample	无异常 No abnormalities		
测试周期 Date of testing	2024.11.16-2024.11.22		
结论 Test Conclusion	本报告仅提供实测值。详见本报告测试结果汇总页。 Only measured values are provided in this report. See the test results summary page of this report for details.		
委托单位通讯资料 Entrustment company communicate data	——		
备注 Remarks	——		

编制：徐松若　　审核：　　批准（盖章）：吴雪松

日期：2024.11.22　　日期：2024.11.22　　日期：2024.11.22

分析测试专用章

测 试 报 告

1. 测试条件/ Test condition：

环境温度（Temperature）：24.7 ℃

湿度（Humidity）：52.4% RH

辐照度（Irradiance）：1000 W/m^2

2. 光电性能参数/ Photoelectric performance parameter：

序号/NO.	测试项目/Test item	单位 /Unit	测试结果/ Test result	备注/Remarks
1	器件面积（Device area）	cm^2	1.00	/
2	开路电压 V_{OC}（Open circuit voltage）	V	0.916	/
3	短路电流密度 J_{SC}（Short circuit current density）	mA/cm^2	27.06	/
4	填充因子 *FF*（Fill factor）	%	73.97	/
5	光电转化效率 PCE（Efficiency）	%	18.35	/

3. 电流-电压曲线（I-V curve）：

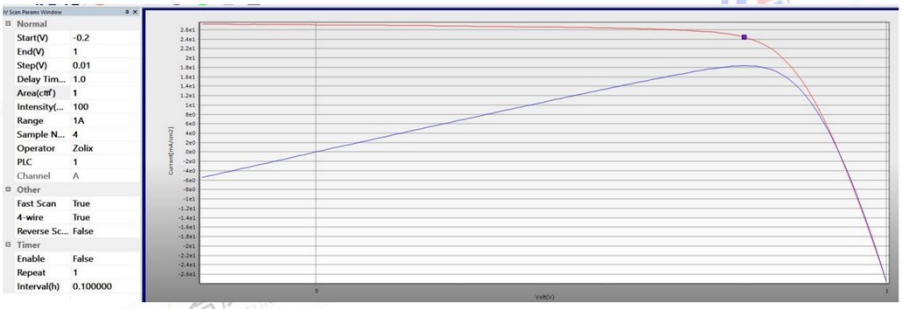

4. 器件照片（**Device photograph**）：

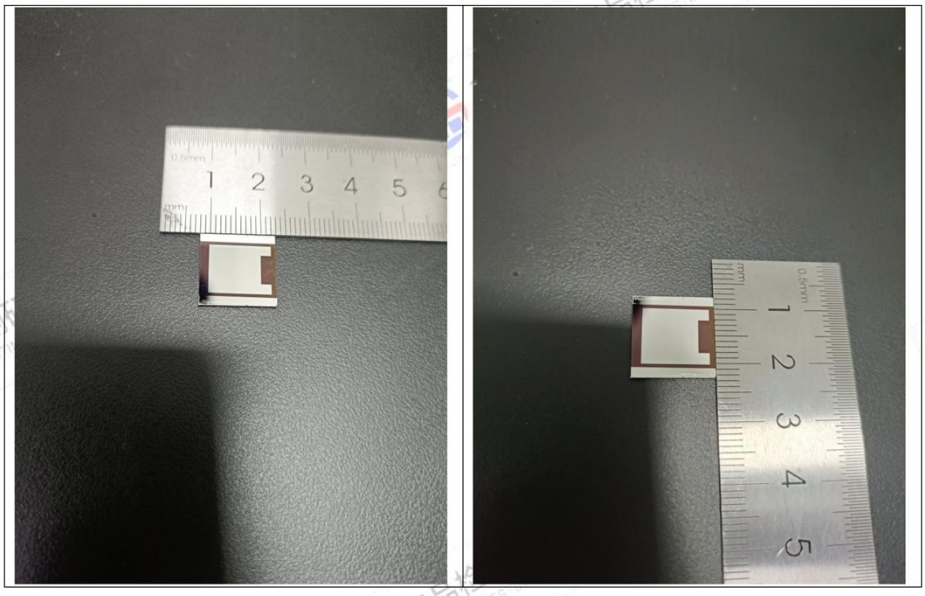

**********报告结束**********

Fig. S3. The certificate report of the D18:PTzBI-dF:L8-BO (0.5:0.5:1) 1 cm^2 OPV device by the Hefei Guangce Product Testing Institute.

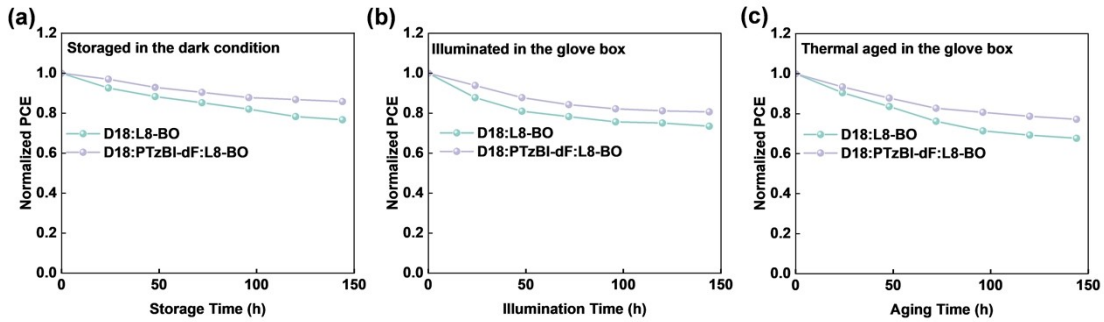

Fig. S4. (a) Normalized PCE as a function of storage time for D18:L8-BO (1:1) and D18:PTzBI-dF:L8-BO (0.5:0.5:1) devices in dark conditions. (b) Normalized PCE as a function of illumination time for D18:L8-BO (1:1) and D18:PTzBI-dF:L8-BO (0.5:0.5:1) devices under LED illumination. (c) Normalized PCE as a function of thermal-aging time for D18:L8-BO (1:1) and D18:PTzBI-dF:L8-BO (0.5:0.5:1) devices at 80 °C.

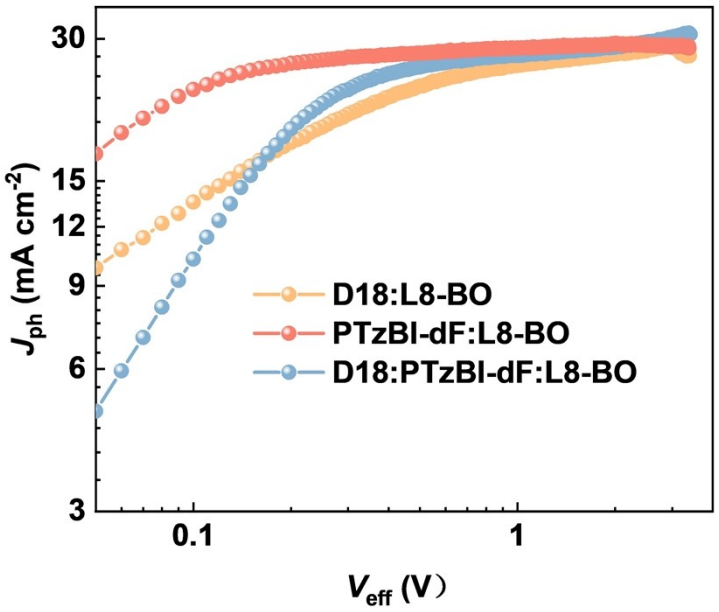

Fig. S5. (a) J_{ph}-V_{eff} curves of D18:L8-BO (1:1), PTzBI-dF:L8-BO (1:1) and D18:PTzBI-dF:L8-BO (0.5:0.5:1) OPV devices.

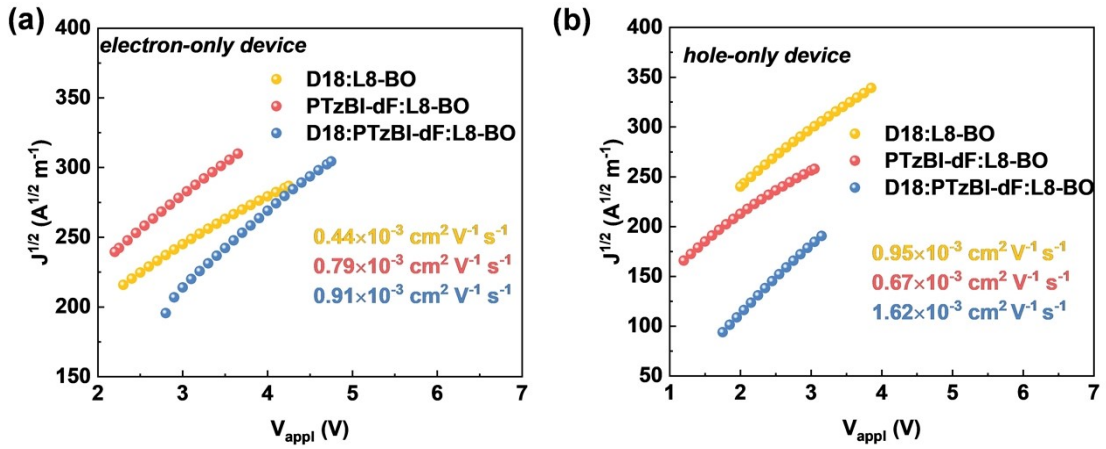

Fig. S6. $J^{1/2}$-V plots of the SCLC region of (a) hole-only and (b) electron-only devices for D18:L8-BO (1:1), PTzBI-dF:L8-BO (1:1) and D18:PTzBI-dF:L8-BO (0.5:0.5:1) blends.

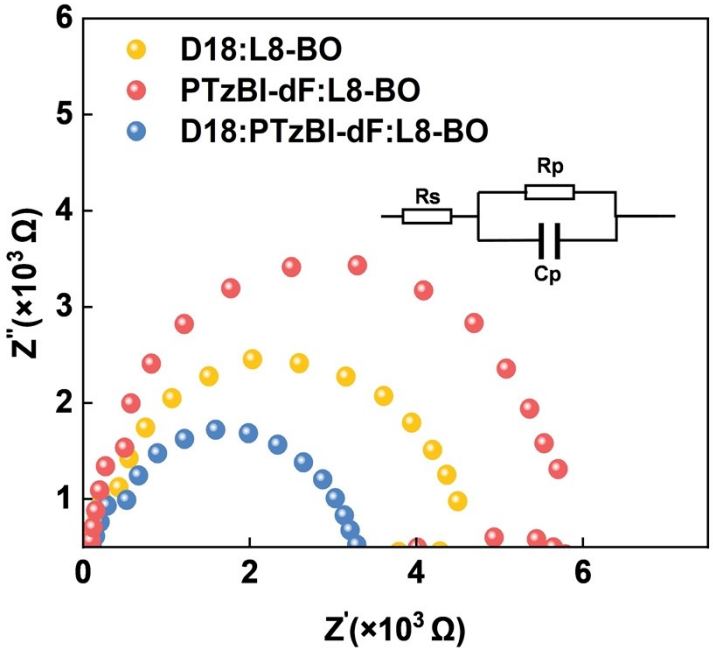

Fig. S7. Impedance spectra of D18:L8-BO (1:1), PTzBI-dF:L8-BO (1:1) and D18:PTzBI-dF:L8-BO (0.5:0.5:1) OPV devices.

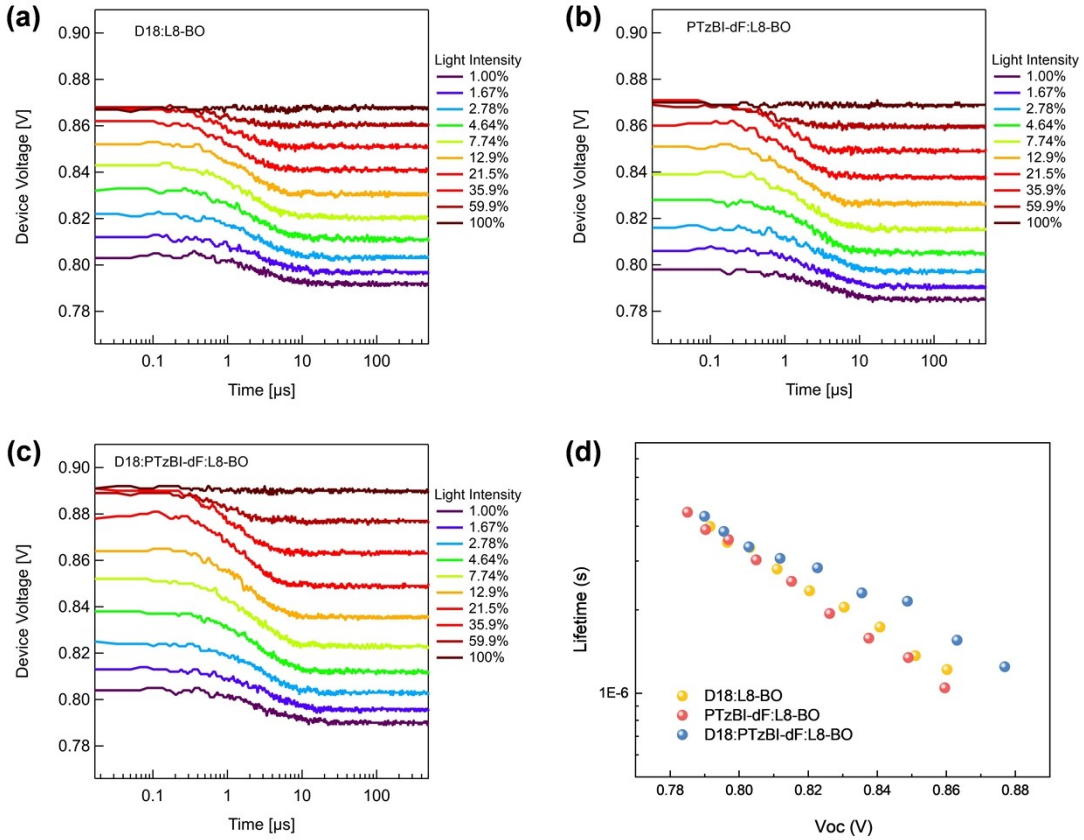

Fig. S8. TPV curves under varying light intensities of (a) D18:L8-BO device, (b) PTzBI-dF:L8-BO device, and (c) D18:PTzBI-dF:L8-BO device. (d) TPV lifetime versus open-circuit voltage of the devices.

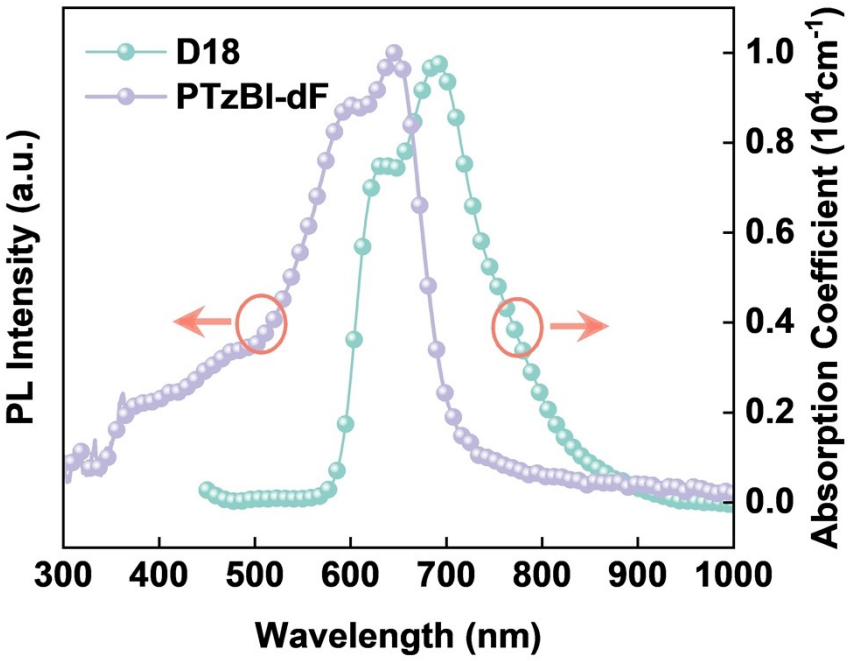

Fig. S9. PL spectrum of D18 and absorption spectrum of PTzBI-dF films.

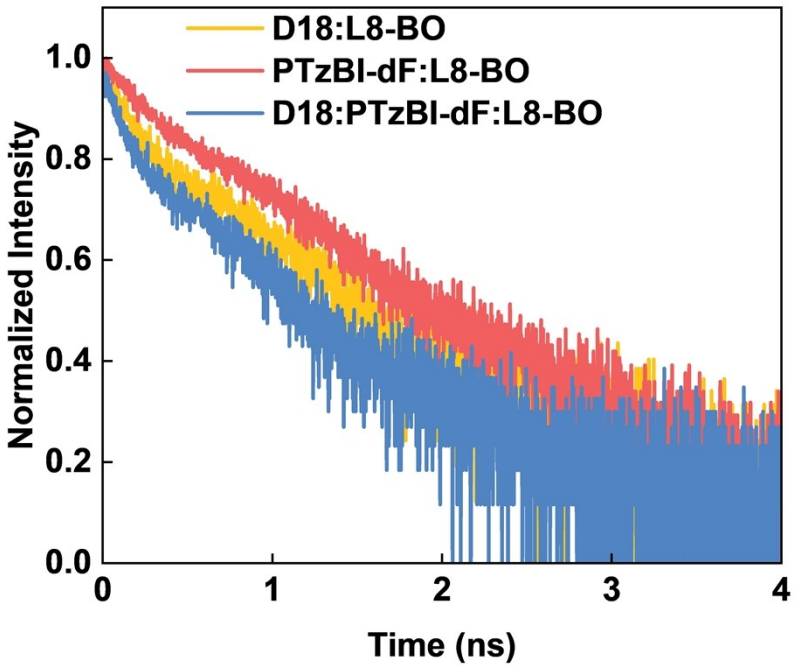

Fig. S10. TRPL characteristics of D18:L8-BO (1:1), PTzBI-dF:L8-BO (1:1) and D18:PTzBI-dF:L8-BO (0.5:0.5:1) films.

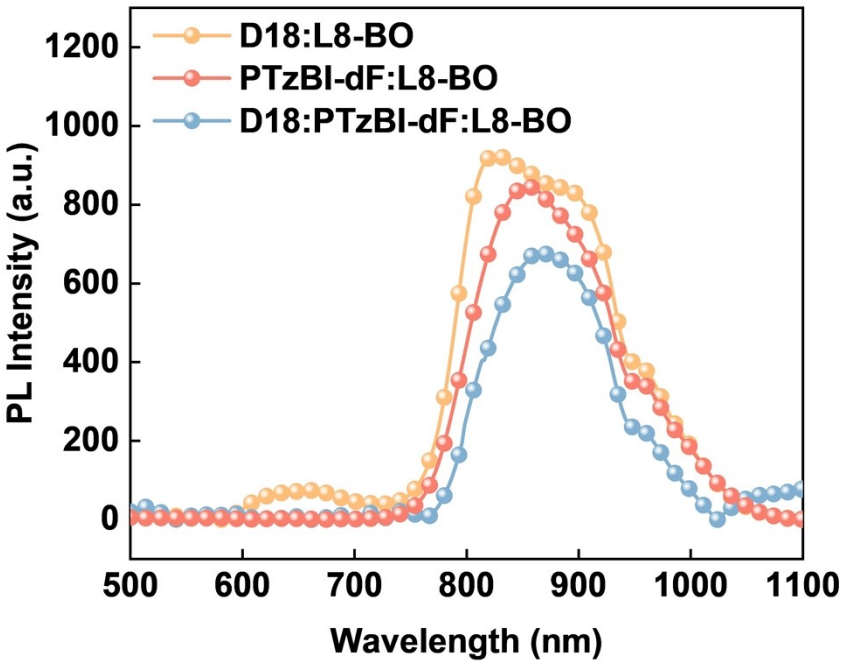

Fig. S11. PL spectra of D18:L8-BO (1:1), PTzBI-dF:L8-BO (1:1) and D18:PTzBI-dF:L8-BO (0.5:0.5:1) films.

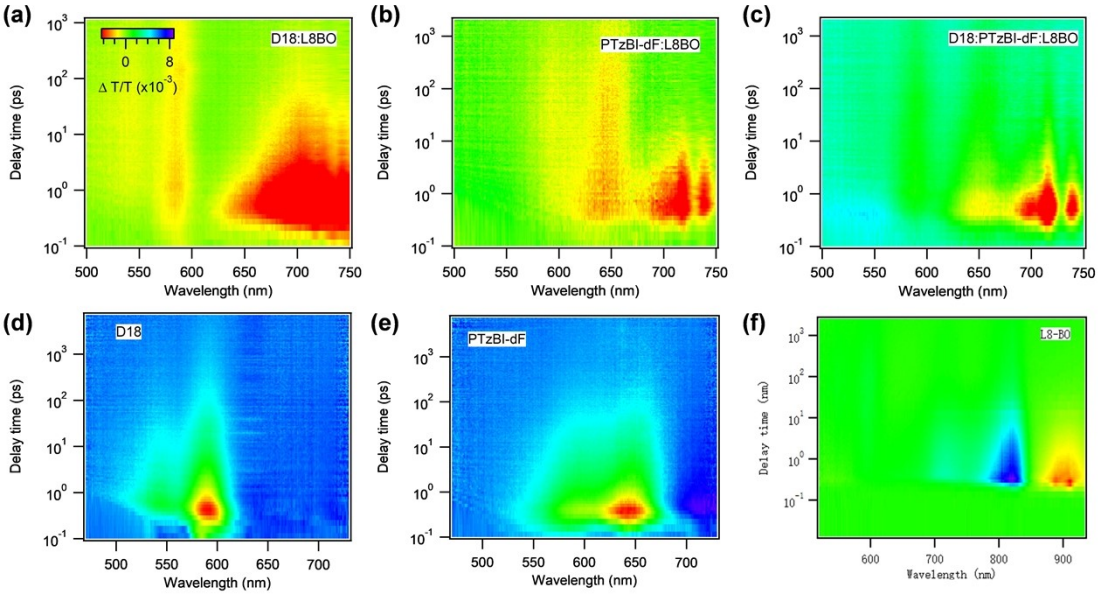

Fig. S12. The contour plots of transient absorption (TA) spectra of (a) D18:L8-BO, (b) PTzBI-dF:L8-BO and (c) D18:PTzBI-dF:L8-BO blend films (800 nm excited) and neat (d) D18 (520 nm excited), (e) PTzBI-dF (520 nm excited), and (f) L8-BO films (800 nm excited).

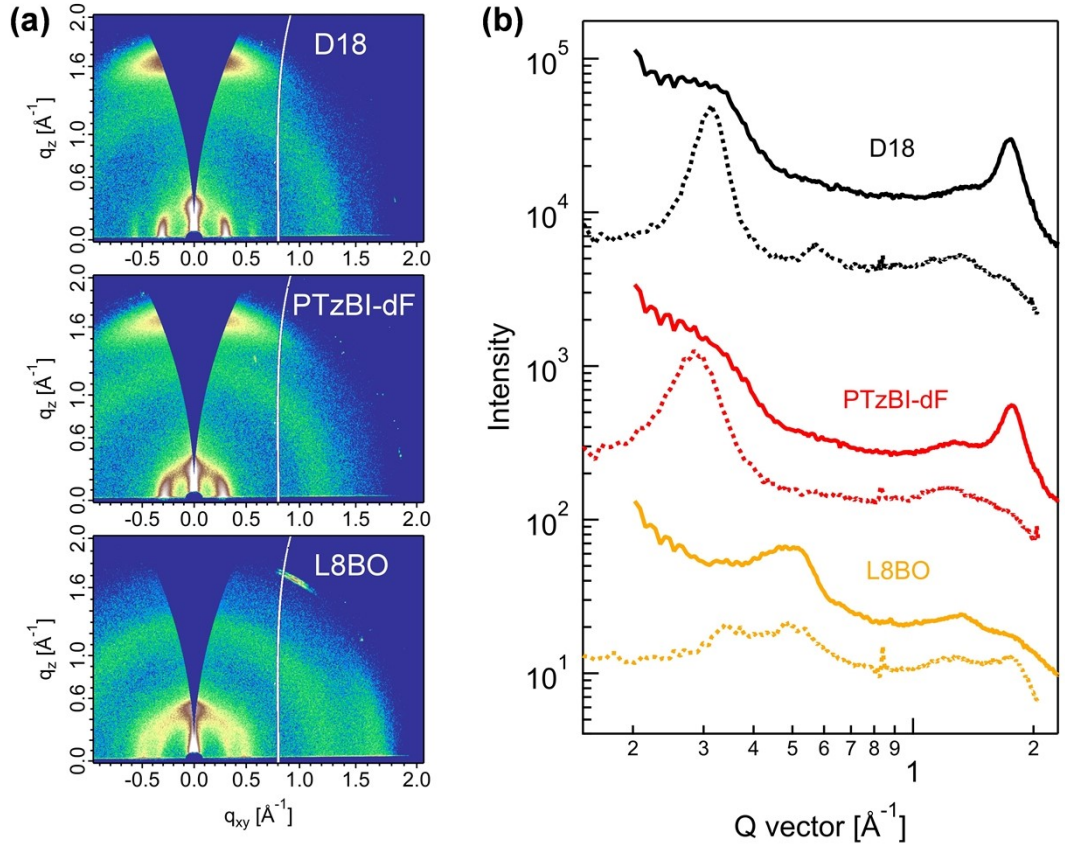

Fig. S13. GIWAXS (a) images and (b) averaged I-q curves in the IP (dotted lines) and OOP (solid lines) directions of neat films.

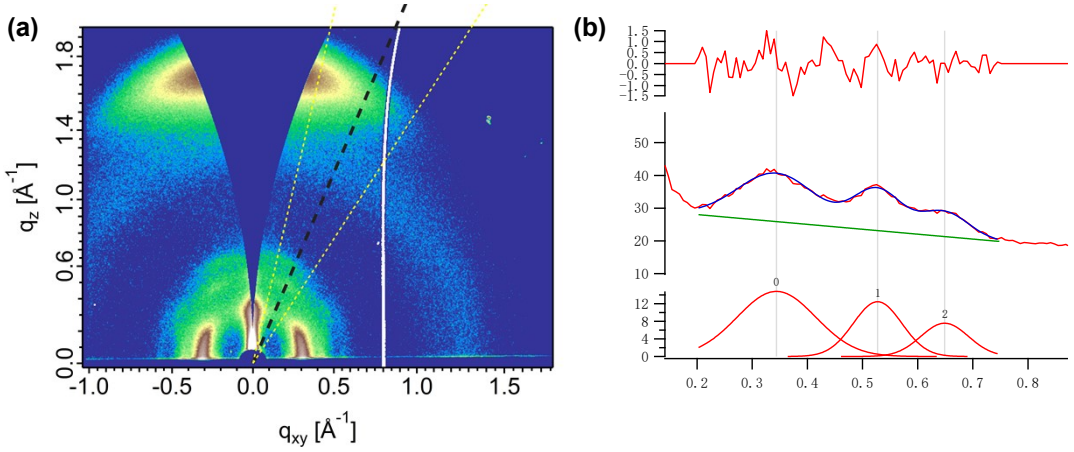

Fig. S14. (a) Sector averaging of the 2D GIWAXS image at the azimuthal angle of 67°. (b) Multi-peak fitting to the resultant I-q curve with Gaussian functions, showing the (021) peak at 0.53 Å^{-1}.

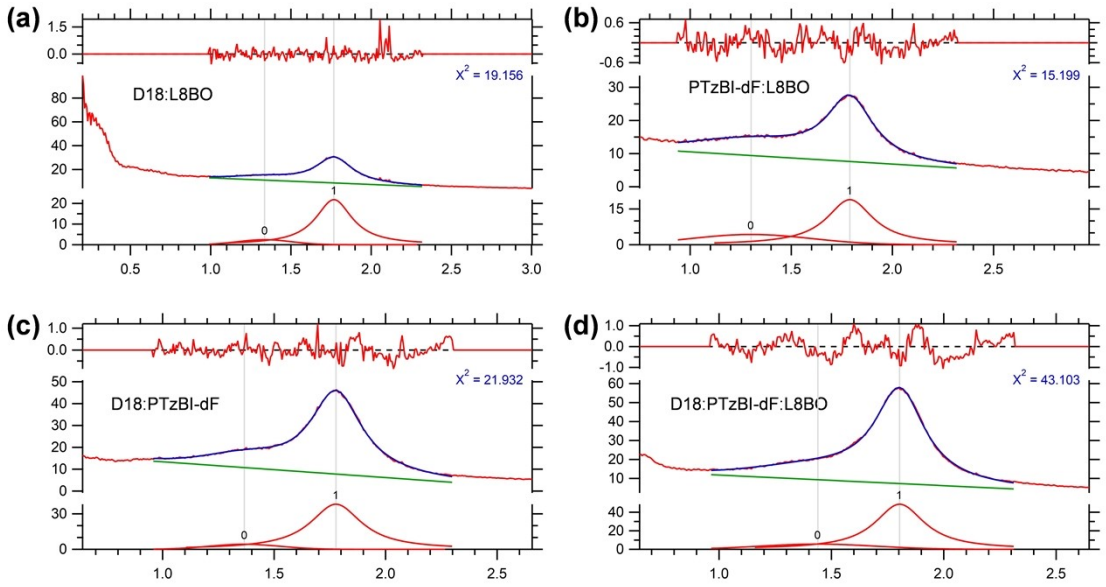

Fig. S15. Fitting results of GIWAXS averaged I-q curves in the OOP direction of blend films, yielding the packing parameters related to π-π stacking.

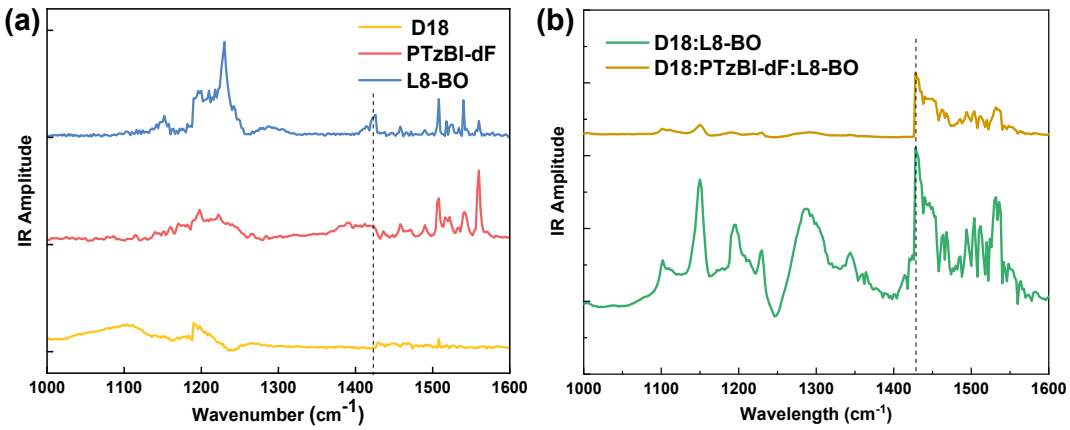

Fig. S16. IR spectra of neat and blend films. The dotted line at 1430 cm^{-1} can be used to highlight L8-BO within the D18/PTzBI-dF matrix.

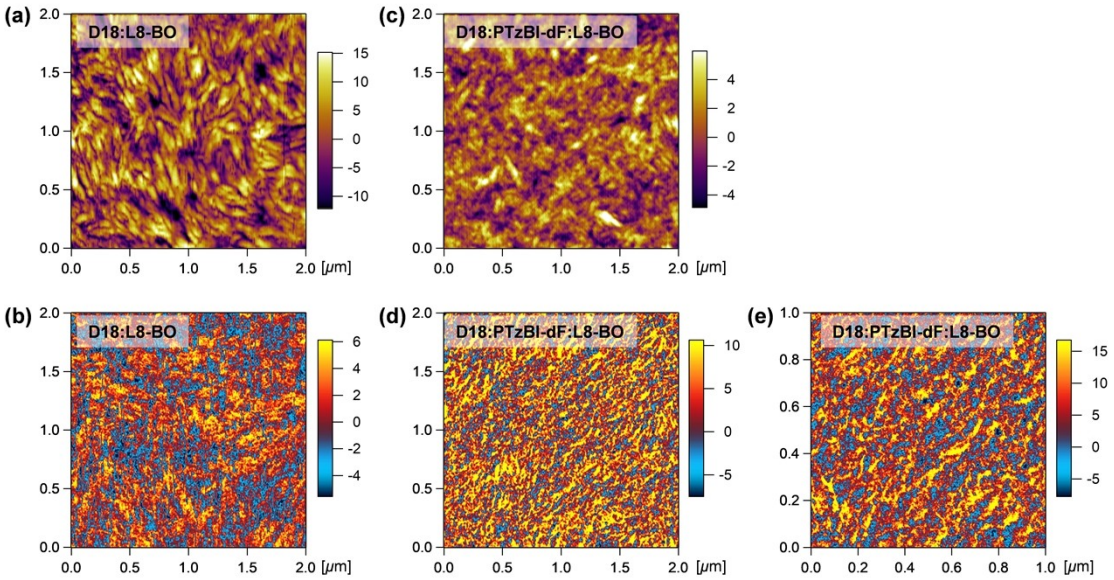

Fig. S17. AFM-IR images (probed at 1430 cm^{-1}) of D18:L8-BO and D18:PTzBI-dF:L8-BO blend films: (a, c) height images (2 μm × 2 μm) and (b, d) IR amplitude images (2 μm × 2 μm). (e) Magnitude image corresponding to (d), with a size of 1 μm × 1 μm. The color bar for the height images is in nanometers, while the color bar for the AFM-IR images represents amplitude.

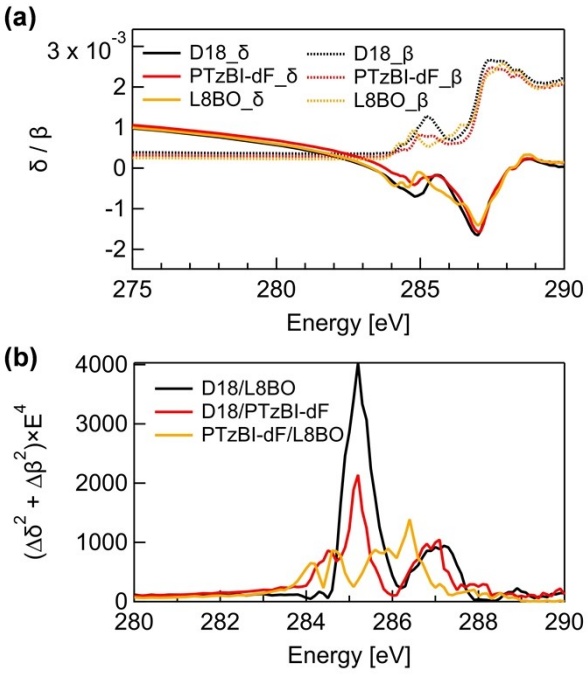

Fig. S18. (a) Refractive indices and (b) scattering contrast functions at C K-edge of D18, PTzBI-dF, and L8-BO.

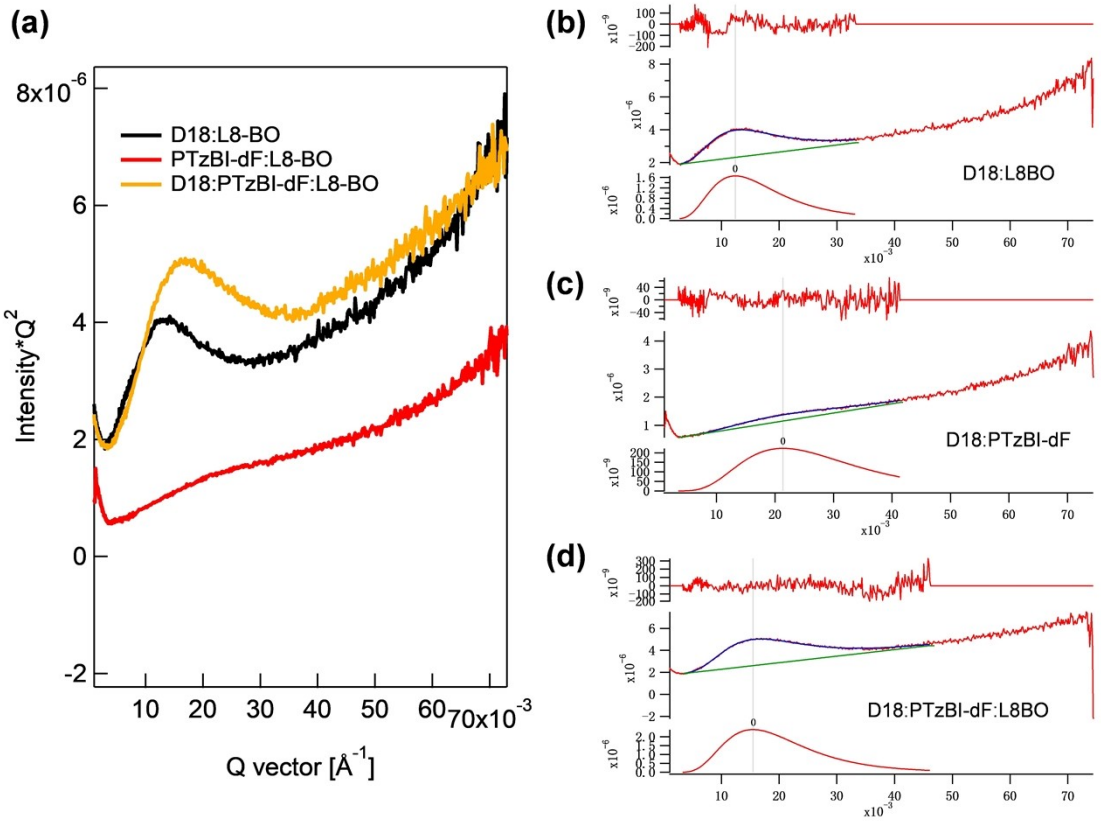

Fig. S19. (a) RSoXS Iq2-q curves at 285.2 eV and (b) fitted results with log-normal functions of D18:L8-BO (1:1), PTzBI-dF:L8-BO (1:1), and D18:PTzBI-dF:L8-BO (0.5:0.5:1) blend films.

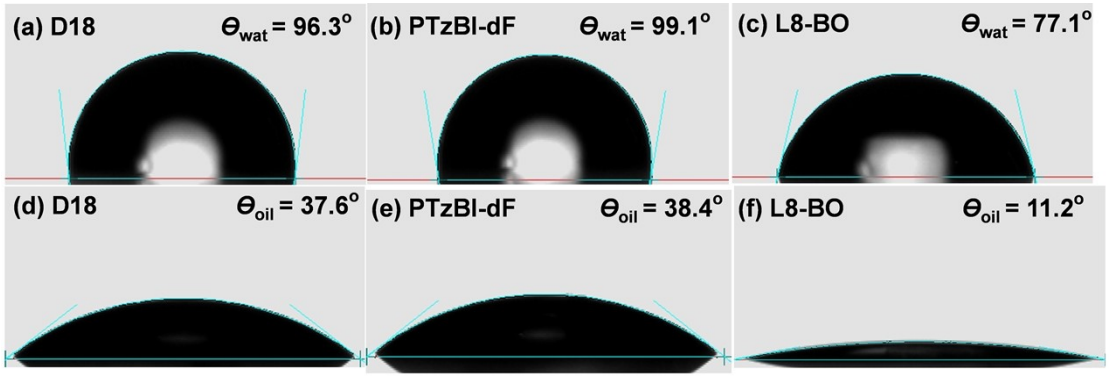

Fig. S20. Images of surface contact angle measurements for (a, d) neat D18, (b, e) neat PTzBI-dF, and (c, f) neat L8-BO films.

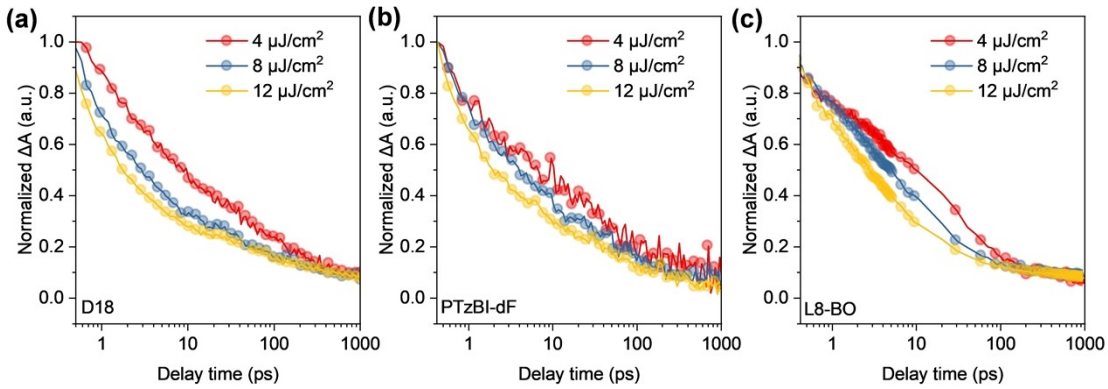

Fig. S21. The TA kinetics of the excitons in the neat films at indicated excitation fluences: (a) D18 (520 nm excited); (b) PTzBI-dF (520 nm excited); (c) L8-BO (800 nm excited).

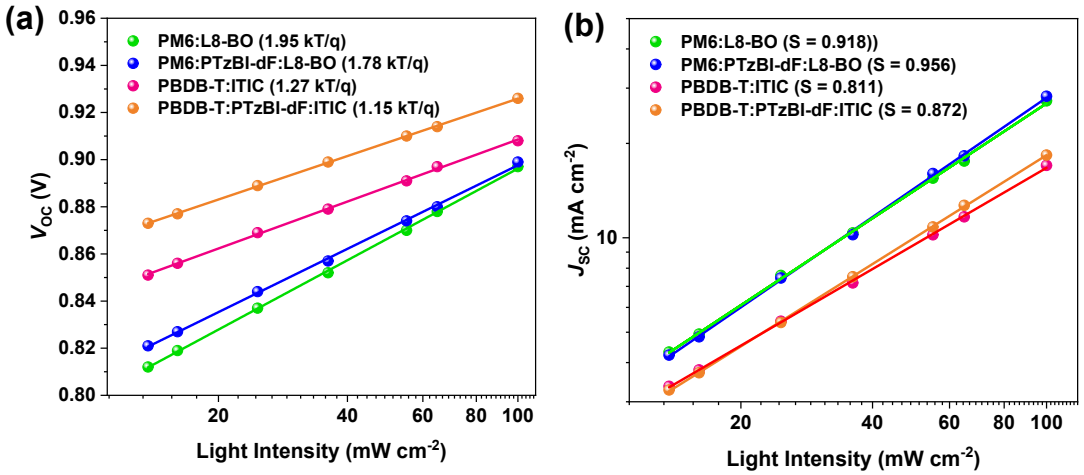

Fig. S22. Light-intensity dependence of (a) V_{OC} and (b) J_{SC} characteristics for devices based on PM6:L8-BO and PBDB-T:ITIC blends with and without PTzBI-dF.

Table S1. Photovoltaic parameters of D18:PTzBI-dF:L8-BO devices with different donor blend ratios.

Active layer	Blend ratio (wt:wt:wt)	V_{OC} (V)	J_{SC} (mA cm^{-2})	FF (%)	PCE (%)
D18:PTzBI-dF:L8-BO [a]	1:0:1	0.89	27.14	70.24	16.97
	0.75:0.25:1	0.89	27.28	71.02	17.24
	0.5:0.5:1	0.89	27.76	71.85	17.75
	0.25:0.75:1	0.89	27.64	70.36	17.31
	0:1:1	0.89	27.59	69.53	17.07

[a] The blend films were processed by CF without solvent additive and post-treated with 100 °C for 5 min.

Table S2. Photovoltaic parameters of D18:PTzBI-dF:L8-BO devices with different L8-BO addition.

Active layer	Blend ratio (wt:wt:wt)	V_{OC} (V)	J_{SC} (mA cm^{-2})	FF (%)	PCE (%)
D18:PTzBI-dF:L8-BO [a]	0.5:0.5:0.8	0.89	27.02	72.33	17.39
	0.5:0.5:1	0.89	27.76	71.85	17.75
	0.5:0.5:1.2	0.89	27.98	71.01	17.68
	0.5:0.5:1.5	0.89	28.15	69.12	17.32

[a] The blend films were processed by CF without solvent additive and post-treated with 100 °C for 5 min.

Table S3. Photovoltaic parameters of D18:PTzBI-dF:L8-BO (0.5:0.5:1) devices with the active layers processed by various solvents.

Active layer	Solvent	V_{OC} (V)	J_{SC} (mA cm^{-2})	FF (%)	PCE (%)
D18:PTzBI-dF:L8-BO [a]	CF	0.89	27.76	71.85	17.75
	CB	0.89	22.35	72.96	14.51
	o-DCB	0.89	21.22	72.67	13.72

[a] The blend films were post-treated with 100 °C for 5 min.

Table S4. Photovoltaic parameters of CF processed D18:PTzBI-dF:L8-BO (0.5:0.5:1) devices with various solvent additives.

Active layer	Solvent additive	V_{OC} (V)	J_{SC} (mA cm^{-2})	FF (%)	PCE (%)
D18:PTzBI-dF:L8-BO [a]	N/A	0.89	27.76	71.85	17.75
	0.3% CN	0.90	27.82	75.36	18.94
	0.5% CN	0.90	27.84	78.42	19.64
	1% CN	0.89	27.88	78.89	19.57
	0.5% DBE	0.89	28.44	76.13	19.27
	0.5% DIO	0.89	28.26	77.05	19.38

[a] The blend films were post-treated with 100 °C for 5 min.

Table S5. Photovoltaic parameters of D18:PTzBI-dF:L8-BO (0.5:0.5:1) devices with active layer thermal annealed at different temperatures.

Active layer	Thermal annealing	V_{OC} (V)	J_{SC} (mA cm^{-2})	FF (%)	PCE (%)
D18:PTzBI-dF:L8-BO [a]	As-cast	0.89	27.63	68.16	16.76
	90 °C /5min	0.90	27.69	77.63	19.35
	100 °C /5min	0.90	27.84	78.42	19.64
	110 °C /5min	0.90	27.47	78.11	19.31
	120 °C /5min	0.90	27.30	77.67	19.08

[a] The blend films were processed by CF with 0.5 vol% CN.

Table S6. Photovoltaic parameters of single-junction OPVs with efficiency over 19% reported in the literature.

Active layer	V_{OC} (V)	J_{SC} (mA cm^{-2})	FF (%)	PCE (%)	Ref.
D18:AQx-18:L8-BO	0.928	25.90	79.20	19.10	5
BTP-FTh:IDIC (0.8:0.2)	0.870	27.17	80.60	19.05	6
PBQx-TF:eC9-2Cl:F-BTA	0.879	26.70	80.9	19.00	7
PM6:BTP-eC9:$PC_{71}BM$	0.860	27.62	80.00	19.03	8
PBDB-TF:BTP-eC11	0.832	13.40	77.06	19.75	9
PM6:PY-IT	0.898	26.17	80.87	19.01	10
PM6:L8-BO:Tet-1 (10%)	0.887	26.98	80.70	19.31	11
D18:PM6:Z9	0.896	26.50	80.10	19.00	12
PM6:L8-BO	0.862	28.50	78.06	19.18	13
PM6:BTP-eC9:BTP-BO-3FO	0.857	28.13	79.80	19.24	14
PM6:Dimer-2CF	0.900	26.39	80.03	19.02	15
PM6:L8-BO+0.2% T-2OEH	0.888	26.90	80.40	19.20	16

PM6:L8-BO+BDT	0.893	26.59	80.03	19.01	17
D18:N3:DP-BTP	0.870	27.95	78.50	19.07	18
PBTz-F:PM6:L8-BO	0.888	27.30	79.50	19.43	19
DL1:Y6	0.869	27.82	78.94	19.10	20
D18-Cl:L8-BO-X	0.893	26.78	79.60	19.04	21
L8-BO:HW-D18	0.910	26.48	80.65	19.65	22
BTIC-C9-4Cl:L8-BO	0.870	26.98	80.67	19.01	23
PM6:D18:CH-FB	0.888	26.69	80.03	18.97	24
PM6:L8-BO	0.902	26.98	79.41	19.32	25
PBDB-T:ITIC:$PC_{71}BM$	0.846	28.10	80.40	19.11	26
PM6 + 10% INMB-F/L8-BO	0.883	26.94	81.30	19.40	27
D18:BTP-eC9-4F:2TT	0.880	27.29	79.67	19.39	28
PM6:L8-BO	0.890	26.65	80.92	19.25	29
D18:D18-Cl:CH8F	0.909	26.81	79.10	19.28	30
PM6:BTP-eC9:$PC_{71}BM$	0.860	27.62	80.00	19.03	31
D18:DTC11	0.858	27.50	80.50	19.00	32
PM6:BTP-eC9:L8-BO/FPA	0.884	26.96	80.45	19.20	33
PM6:Y6:SF-BTA1	0.870	27.30	80.50	19.10	34
PM6:PM6-PA:L8-BO	0.880	27.00	80.80	19.30	35
PM6:L8-BO:bi-asy-YC12	0.897	27.17	78.90	19.23	36
PM6:PY-IT	0.945	26.37	76.48	19.06	37
PM6:L8-BO:BTP-ThMeCl	0.870	26.70	82.20	19.10	38
D18:AQx-18:L8-BO	0.928	25.90	79.20	19.10	39
PM6:BTP-eC9:L8-BO-X	0.883	27.70	80.10	19.60	40
PB2:FTCC-Br:BTP-eC9	0.888	26.90	81.60	19.50	41
PB2:HLG:BTP-eC9	0.883	27.30	80.80	19.50	42
D18:L8-BO(DIB)	0.907	26.00	78.7	19.60	43
PM6:L8-BO(PyMC5)	0.904	27.25	79.10	19.52	44

Table S7. Photovoltaic parameters of 1 cm^2 single-junction OPVs reported in the literatures.

Device area (cm^2)	V_{OC} (V)	J_{SC} (mA cm^{-2})	FF (%)	PCE (%)	Ref.
1 cm^2	0.890	19.22	62.19	10.65	[45]
	0.881	21.26	62.00	11.61	[46]
	0.797	22.61	71.05	12.80	[47]
	0.831	26.72	68.19	15.13	[48]
	0.869	27.83	66.60	16.10	[49]
	0.846	26.80	72.90	16.50	[50]
	0.821	26.75	75.30	16.54	[51]
	0.850	27.57	74.13	17.37	[52]
	0.857	27.01	75.70	17.52	[53]
	0.890	25.73	76.68	17.55	[54]
	0.869	28.71	71.18	17.76	[55]
	0.916	27.06	73.97	18.35	This work (Certified)

Table S8. Photovoltaic parameters of D18:L8-BO (1:1) and D18:PTzBI-dF:L8-BO (0.5:0.5:1) devices stored in dark conditions for various durations.

Active layer	Storage time (hours)	V_{OC} (V)	J_{SC} (mA cm^{-2})	FF (%)	PCE (%)
D18:L8-BO	0	0.89	27.2	78.2	18.9
	24	0.89	27.1	72.5	17.5
	48	0.89	27.0	69.4	16.7
	72	0.88	26.8	68.2	16.1
	96	0.88	26.4	66.7	15.5
	120	0.88	26.2	64.3	14.8

	144	0.88	26.0	63.5	14.5
D18:PTzBI-dF:L8-BO	0	0.89	28.0	79.1	19.7
	24	0.89	27.9	76.9	19.1
	48	0.89	27.8	73.8	18.3
	72	0.88	27.8	71.8	17.8
	96	0.88	27.7	70.2	17.3
	120	0.88	27.6	69.4	17.1
	144	0.88	27.7	68.7	16.9

Table S9. Photovoltaic parameters for D18:L8-BO (1:1) and D18:PTzBI-dF:L8-BO (0.5:0.5:1) devices continuously illuminated by white LED for different durations.

Active layer	Illumination time (hours)	V_{OC} (V)	J_{SC} (mA cm^{-2})	FF (%)	PCE (%)
D18:L8-BO	0	0.89	27.2	78.2	18.9
	24	0.89	26.3	70.8	16.6
	48	0.89	25.6	67.1	15.3
	72	0.89	25.2	66.0	14.8
	96	0.88	25.0	65.2	14.3
	120	0.88	24.9	64.7	14.2
	144	0.88	24.7	64.1	13.9
D18:PTzBI-dF:L8-BO	0	0.89	28.0	79.1	19.7
	24	0.89	27.4	75.7	18.5
	48	0.89	27.0	72.2	17.3
	72	0.88	26.8	70.3	16.6
	96	0.88	26.7	69.0	16.2
	120	0.88	26.7	68.1	16.0
	144	0.88	26.6	67.8	15.9

Table S10. Photovoltaic parameters for D18:L8-BO (1:1) and D18:PTzBI-dF:L8-BO (0.5:0.5:1) devices thermal-aged at 80 °C for different durations.

Device	Thermal-aged time (hours)	V_{OC} (V)	J_{SC} (mA cm^{-2})	FF (%)	PCE (%)
D18:L8-BO	0	0.89	27.2	78.2	18.9
	24	0.88	26.7	72.8	17.1
	48	0.88	26.2	68.4	15.8
	72	0.88	25.7	63.8	14.4
	96	0.88	24.9	61.4	13.5
	120	0.88	24.5	60.6	13.1
	144	0.88	24.2	60.1	12.8
D18:PTzBI-dF:L8-BO	0	0.89	28.0	79.1	19.7
	24	0.89	27.6	74.9	18.4
	48	0.88	27.5	71.4	17.3
	72	0.88	27.1	68.3	16.3
	96	0.88	26.6	67.9	15.9
	120	0.88	26.3	67.1	15.5
	144	0.88	26.1	66.2	15.2

Table S11. Results of J_{ph}-V_{eff} curves for D18:L8-BO (1:1), PTzBI-dF:L8-BO (1:1), and D18:PTzBI-dF:L8-BO (0.5:0.5:1) OPV devices.

Active layer	J_{ph} (mA cm^{-2})	J_{sat} (mA cm^{-2})	G_{max} (m^{-3} s^{-1})	*P(E, T)*
D18:L8-BO	25.76	28.33	1.77×10^{28}	0.909
D18:PTzBI-dF:L8-BO	27.52	28.46	1.78×10^{28}	0.968
PTzBI-dF:L8-BO	25.51	27.14	1.70×10^{28}	0.939

Table S12. SCLC electron and hole mobilities extracted from D18:L8-BO (1:1), PTzBI-dF:L8-BO (1:1) and D18:PTzBI-dF:L8-BO (0.5:0.5:1) charge-only devices.

Active layer	μ_h (cm^2 V^{-1} s^{-1})	μ_e (cm^2 V^{-1} s^{-1})	Thickness (nm)
D18:L8-BO	0.95×10^{-3}	0.44×10^{-3}	~100
D18:PTzBI-dF:L8-BO	1.62×10^{-3}	0.91×10^{-3}	~100
PTzBI-dF:L8-BO	0.67×10^{-3}	0.79×10^{-3}	~100

Table S13. Surface contact angle, surface energy, interfacial tension, wetting coefficient, and Flory-Huggins interaction parameters of D18, PTzBI-dF and L8-BO.

Film [a]	Θ_{wat} (°)	Θ_{oil} (°)	γ_d [b] (mN m^{-1})	γ_p [b] (mN m^{-1})	γ (mN m^{-1})	Interfacial tension [c] (γ_{AB})	Wetting coefficient [d] (ω)	Flory-Huggins interaction parameter [e] (χ)
D18	96.3	37.6	42.87	0.21	43.08	γ_{AB} = 0.01	/	χ_{AB} = 0.01
PTzBI-dF	99.1	38.4	43.16	0.62	43.78	γ_{BC} = 0.58	ω_B = 0.78	χ_{BC} = 0.67
L8-BO	77.1	11.2	48.71	1.10	49.81	γ_{AC} = 0.73	/	χ_{AC} = 0.84

[a] A = D18, B = PTzBI-dF, C = L8-BO; [b] γ_d and γ_p represent the surface free energies generated from the dispersion forces and the polar forces, respectively; [c] Calculated from Neumann's equation $\gamma_{AB} = \gamma_A + \gamma_B - 2(\gamma_A\gamma_B)^{1/2}e^{\wedge}{-}\beta(\gamma_A{-}\gamma_B)^2$, where β = 0.000115 m^4 m J^{-2}; [d] The wetting coefficient component B in the blends of A and C can be expressed according to the Young's equation: $\omega_B = (\gamma_{BC} - \gamma_{AB})/\gamma_{AC;}$ [e] χ_{AB} was obtained from the equation $\chi_{AB} = V_0(K\gamma_A^{1/2} - K\gamma_B^{1/2})^2/(RT)$, where K stands for the proportional constant ($K = 116 \times 10^3$ m$^{-1/2}$), V_0 stands for the geometric average molar volume, γ stands for the surface energies of materials A and B, R stands for the gas constant and T stands for the absolute temperature.

Table S14. Photovoltaic parameters of OPV devices based on PM6:L8-BO and PBDB-T:ITIC blends with and without PTzBI-dF.

Active layer (wt:wt)	V_{OC} [a] (V)	J_{SC} [a] (mA cm^{-2})	FF [a] (%)	PCE [a] (%)
PM6:L8-BO (1:1)	0.90 (0.89±0.01)	27.1 (26.8±0.3)	75.7 (75.0±0.7)	18.4 (18.1±0.3)
PM6:PTzBI-dF:L8-BO (0.5:0.5:1)	0.90 (0.89±0.01)	27.8 (27.3±0.5)	78.0 (77.1±0.9)	19.6 (19.2±0.4)
PBDB-T:ITIC (1:1)	0.88 (0.87±0.01)	17.1 (16.9±0.2)	69.5 (69.1±0.4)	10.4 (10.1±0.3)
PBDB-T:PTzBI-dF:ITIC (0.5:0.5:1)	0.90 (0.89±0.01)	18.4 (17.8±0.6)	70.9 (70.6±0.3)	11.7 (11.5±0.2)

[a] The statistical parameters were calculated from 10 devices.

References

1 Blom, P. W. M., Mihailetchi, V. D., Koster, L. J. A. & Markov and D. E. *Adv. Mater.*, **2007**, *19*, 1551-1566.

2 G. Zhou, M. Zhang, J. Xu, Y. Yang, T. Hao, L. Zhu, L. Zhou, H. Zhu, Y. Zou, G. Wei, Y. Zhang and F. Liu, *Energy Environ. Sci.*, **2022**, *15*, 3483.

3 S. Chandrabose, K. Chen, A. J. Barker, J. J. Sutton, S. K. K. Prasad, J. Zhu, J. Zhou, K. C. Gordon, Z. Xie, X. Zhan and J. M. Hodgkiss, *J. Am. Chem. Soc.*, **2019**, *141*, 6922-6929.

4 J. Ilavsky, *J. Appl.*, *Crystallogr.*, **2012**, *45*, 324-328.

5 R. Sun, Y. Wu, X. Yang, Y. Gao, Z. Chen, K. Li, J. Qiao, T. Wang, J. Guo, C. Liu, X. Hao, H. Zhu and J. Min, *Adv. Mater.*, **2022**, *34*, 2110147.

6 K. Chong, X. Xu, H. Meng, J. Xue, L. Yu, W. Ma and Q. Peng, *Adv. Mater.*, **2022**, *34*, 2109516.

7 Y. Cui, Y. Xu, H. Yao, P. Bi, L. Hong, J. Zhang, Y. Zu, T. Zhang, J. Qin, J. Ren, Z. Chen, C. He, X. Hao, Z. Wei and J. Hou, *Adv. Mater.*, **2021**, *33*, 2102420.

8 L. Zhu, M. Zhang, J. Xu, C. Li, J. Yan, G. Zhou, W. Zhong, T. Hao, J. Song, X. Xue, Z. Zhou, R. Zeng, H. Zhu, C. Chen, R. MacKenzie, Y. Zou, J. Nelson, Y. Zhang, Y. Sun and F. Liu, *Nat. Mater.*, **2022**, *21*, 656−663.

9 J. Wang, Z. Zheng, Y. Zu, Y. Wang, X. Liu, S. Zhang, M. Zhang and J. Hou, *Adv. Mater.*, **2021**, *33*, 2102787.

10 Z. Wang, H. Wang, M. Du, X. Lai, F. He, Q. Guo, Q. Guo, A. Tang, X. Sun and E. Zhou, *Adv. Funct. Mater.*, **2024**, *34*, 2313240.

11 C. Zhang, J. Song, L. Ye, X. Li, M. H. Jee, H. Y. Woo and Y. Sun, *Angew. Chem. Int. Ed.*, **2024**, *63*, e202316295.

12 F. Liu, Y. Jiang, R. Xu, W. Su, S. Wang, Y. Zhang, K. Liu, S. Xu, W. Zhang, Y. Yi, W. Ma and X. Zhu, *Angew. Chem. Int. Ed.*, **2024**, *63*, e202313791.

13 G. Zhang, Q. Chen, Z. Zhang, Z. Gao, C. Xiao, Y. Wei and W. Li, *Adv. Mater.*, **2024**, *36*, 2310630.

14 B. Zou, W. Wu, T. A. D. Peña, R. Ma, Y. Luo, Y. Hai, X. Xie, M. Li, Z. Luo, J. Wu, C. Yang, G. Li and H. Yan, *Nano-Micro Lett.*, **2024**, *16*, 30.

15 M. Lv, Q. Wang, J. Zhang, Y. Wang, Z.-G. Zhang, T. Wang, H. Zhang, K. Lu, Z. Wei and D. Deng, *Adv. Mater.*, **2024**, *36*, 2310046.

16 C. Liu, Y. Fu, J. Zhou, L. Wang, C. Guo, J. Cheng, W. Sun, C. Chen, J. Zhou, D. Liu, W. Li and T. Wang, *Adv. Mater.*, **2024**, *36*, 2308608.

17 M. Dong, S. Chen, L. Hong, J. Jing, Y. Bai, Y. Liang, C. Zhu, T. Shi, W. Zhong, L. Ying, K. Zhang and F. Huang, *Nano Energy*, **2024**, *119*, 109097.

18 X. Liu, Z. Zhang, C. Wang, C. Zhang, S. Liang, H. Fang, B. Wang, Z. Tang, C. Xiao and W. Li, *Angew. Chem. Int. Ed.*, **2024**, *63*, e202316039.

19 Y. Ran, C. Liang, Z. Xu, W. Jing, X. Xu, Y. Duan, R. Li, L. Yu and Q. Peng, *Adv. Funct. Mater.*, **2024**, *34*, 2311512.

20 D. He, J. Zhou, Y. Zhu, Y. Li, K. Wang, J. Li, J. Zhang, B. Li, Y. Lin, Y. He, C. Wang and F. Zhao, *Adv. Mater.*, **2024**, *36*, 2308909.

21 S. Luo, C. Li, J. Zhang, X. Zou, H. Zhao, K. Ding, H. Huang, J. Song, J. Yi, H. Yu, K. S. Wong, G. Zhang, H. Ade, W. Ma, H. Hu, Y. Sun and H. Yan, *Nat. Commun.*, **2023**, *14*, 6964.

22 H. Lu, W. Liu, G. Ran, Z. Liang, H. Li, N. Wei, H. Wu, Z. Ma, Y. Liu, W. Zhang, X. Xu and Z. Bo, *Angew. Chem. Int. Ed.*, **2023**, *62*, e202314420.

23 H. Lai, H. Chen, Z.-Y. Chen, Y. Lang, Y. Zhu, S.-T. Zhang, X. Lai, P. Tan, Y.

Zhang, B. Yang, G. Li and F. He, *Energy Environ. Sci.*, **2023**, *16*, 5944−5955.

24 H. Liang, H. Chen, Y. Zou, Y. Zhang, Y. Guo, X. Cao, X. Bi, Z. Yao, X. Wan and Y. Chen, *Chem. Commun.*, **2023**, *59*, 13367−13370.

25 L. Wen, H. Mao, L. Zhang, J. Zhang, Z. Qin, L. Tan and Y. Chen, *Adv. Mater.*, **2024**, *36*, 2308159.

26 Q. Fan, Q. Xiao, H. Zhang, J. Heng, M. Xie, Z. Wei, X. Jia, X. Liu, Z. Kang, C.-Z. Li, S. Li, T. Zhang, Y. Zhou, J. Huang and Z. Li, *Adv. Mater.*, **2024**, *36*, 2307920.

27 Z. Gan, L. Wang, J. Cai, C. Guo, C. Chen, D. Li, Y. Fu, B. Zhou, Y. Sun, C. Liu, J. Zhou, D. Liu, W. Li and T. Wang, *Nat. Commun.*, **2023**, *14*, 6297.

28 H. Lu, W. Liu, G. Ran, J. Li, D. Li, Y. Liu, X. Xu, W. Zhang and Z. Bo, *Adv. Mater.*, **2024**, *36*, 2307292.

29 X. He, Z.-X. Liu, H. Chen and C.-Z. Li, *Adv. Mater.*, **2024**, *36*, 2306681.

30 Z. Yao, X. Cao, X. Bi, T. He, Y. Li, X. Jia, H. Liang, Y. Guo, G. Long, B. Kan, C. Li, X. Wan and Y. Chen, *Angew. Chem. Int. Ed.*, **2023**, *62*, e202312630.

31 Z. Ling, M. I. Nugraha, W. T. Hadmojo, Y. Lin, S. Y. Jeong, E. Yengel, H. Faber, H. Tang, F. Laquai, A.-H. Emwas, X. Chang, T. Maksudov, M. Gedda, H. Y. Woo, I. McCulloch, M. Heeney, L. Tsetseris and T. D. Anthopoulos, *ACS Energy Lett.*, **2023**, *8*, 4104−4112.

32 Z. Zhong, S. Chen, J. Zhao, J. Xie, K. Zhang, T. Jia, C. Zhu, J. Jing, Y. Liang, L. Hong, S. Zhu, D. Ma and F. Huang, *Adv. Energy Mater.*, **2023**, *13*, 2302273.

33 R. Yu, R. Shi, Z. He, T. Zhang, S. Li, Q. Lv, S. Sha, C. Yang, J. Hou and Z. Tan, *Angew. Chem. Int. Ed.*, **2023**, *62*, e202308367.

34 X. Li, A. Tang, H. Wang, Z. Wang, M. Du, Q. Guo, Q. Guo and E. Zhou, *Angew. Chem. Int. Ed.*, **2023**, *62*, e202308367.

35 C. Guo, Y. Fu, D. Li, L. Wang, B. Zhou, C. Chen, J. Zhou, Y. Sun, Z. Gan, D. Liu, W. Li and T. Wang, *Adv. Mater.*, **2023**, *35*, 2304921.

36 Q. Fan, R. Ma, J. Yang, J. Gao, H. Bai, W. Su, Z. Liang, Y. Wu, L. Tang, Y. Li, Q. Wu, K. Wang, L. Yan, R. Zhang, F. Gao, G. Li and W. Ma, *Angew. Chem. Int. Ed.*, **2023**, *62*, e202308307.

37 R. Zeng, L. Zhu, M. Zhang, W. Zhong, G. Zhou, J. Zhuang, T. Hao, Z. Zhou, L. Zhou, N. Hartmann, X. Xue, H. Jing, F. Han, Y. Bai, H. Wu, Z. Tang, Y. Zou, H. Zhu, C.-C. Chen, Y. Zhang and F. Liu, *Nat. Commun.*, **2023**, *14*, 4148.

38 C. Chen, L. Wang, Y. Sun, Y. Fu, C. Guo, B. Zhou, Z. Gan, D. Liu, W. Li and T.

Wang, *Adv. Funct. Mater.*, **2023**, *33*, 2305765.

39 K. Liu, Y. Jiang, F. Liu, G. Ran, F. Huang, W. Wang, W. Zhang, C. Zhang, J. Hou and X. Zhu, *Adv. Mater.*, **2023**, *35*, 2300363.

40 C. Zhao, Y. Wang, K. Sun, C. Gao, C. Li, Z. Liang, L. Zhu, X. Sun, D. Wu, T. Yang, Z. Tang, P. You, C. Xie, Q. Bai, C. Li, J. Yi, H. Hu, S. Li, H. Yan and G. Zhang, *Mater. Sci. Eng. R: Rep.*, **2024**, *160*, 100828.

41 J. Wang, P. Bi, Y. Wang, Z. Zheng, Z. Chen, J. Qiao, W. Wang, J. Li, C. An, S. Zhang, X. Hao and J. Hou, *CCS Chem.*, **2024***, 6,* 218-229.

42 Y. Wang, S. Zhang, J. Wang, J. Ren, J. Qiao, Z. Chen, Y. Yu, X. Hao and J. Hou, *ACS Energy Lett.*, **2024**, *9*, 2420-2427.

43 Y. Fu, L. Xu, Y. Li, Y. Yang, Y. Guo, G. Cai, P. Chan, Y. Ke, C.-J. Su, U-S. Jeng, P. Chow, J.-S. Kim, M.-C. Tang and X. Lu, *Energy Environ. Sci.*, **2024**, *17*, 8893-8903.

44 H. Zhang, Y. Wang, W. Sun,Y. Zhang, B. Zhang, Y. Ding, Z. Zhang, L. Meng, K. Huang and W. Ma, *Angew.Chem.Int.Ed.*, **2024**, DOI: org/10.1002/anie.202417643.

45 Y. Liu, J. Zhang, C. Tian, Y. Shen, T. Wang, H. Zhang, C. He, D. Qiu, Y. Shi and Z. Wei, *Adv. Funct. Mater.,* **2023**, *33*, 2300778.

46 Y.-F. Shen, H. Zhang, J. Zhang, C. Tian, Y. Shi, D. Qiu, Z. Zhang, K. Lu and Z. Wei, *Adv. Mater.*, **2023**, *35*, 2209030.

47 L. Sang, X. Chen, J. Fang, P. Xu, W. Tian, K. Shui, Y. Han, H. Wang, R. Huang, Q. Zhang, Q. Luo and C.-Q. Ma, *Adv. Funct. Mater.,* **2023**, *33*, 2304824.

48 Y. Xiang, L. Feng, H. Wang, Q. Li, Z. Zhang, L. Yan, B. Xu, J. Hou, *Chin. J. Chem.*, **2024**, *42*, 2285-2292.

49 W. Xue, Z. Liang, Y. Tang, C. Zhao, L. Yan, W. Ma and H. Yan, *Adv. Funct. Mater.*, **2023**, *33*, 2304960.

50 Y. Yang, B. Xu and J. Hou, *Small*, **2024**, *20*, 2306668.

51 Y. Han, Z. Hu, W. Zha, X. Chen, L. Yin, J. Guo, Z. Li, Q. Luo, W. Su and C.-Q. Ma, *Adv. Mater.*, **2022**, *34*, 2110276.

52 H. Xia, Y. Zhang, K. Liu, W. Deng, M. Zhu, H. Tan, P. W K Fong, H. Liu, X. Xia, M. Zhang, T. A. Peña, R. Ma, M. Li, J. Wu, Y. Lang, J. Fu, W.-Y. Wong, X. Lu, W. Zhu and G. Li, *Energy Environ. Sci.*, **2023**,*16*, 6078-6093.

53 Y. Zhang, W. Deng, C. E. Petoukhoff, X. Xia, Y. Lang, H. Xia, H. Tang, H. T. Chandran, S. Mahadevan, K. Liu, P. W. K. Fong, Y. Luo, J. Wu, S.-W. Tsang, F. Laquai, H. Wu, X. Lu, Y. Yang and G. Li, *Joule*, **2024**, *8*, 509-526.

54 E. Feng, C. Zhang, J. Chang, Y. Han, H. Li, Q. Luo, C.-Q. Ma, H.-L. Yip, L. Ding and J. Yang, *Cell Rep. Phys. Sci.*, **2024**, *5*, 101883.

55 G. Du, W. Jiang, N. Zhang, Y. Wang, M. Liu, T. Lei, Y. An, L. Ke, C. Ge, F. R. Lin, A. K.-Y. Jen and H. Yip, *Energy Environ. Sci.*, **2025**, DOI: 10.1039/D4EE04479G.